HHS Public Access

Author manuscript

Clin Cancer Res. Author manuscript; available in PMC 2023 August 22.

Published in final edited form as:

Clin Cancer Res. 2022 October 03; 28(19): 4322–4335. doi:10.1158/1078-0432.CCR-22-0977.

Phenotype, Function, and Clinical Significance of CD26^{+} and CD161^{+}Tregs in Splenic Marginal Zone Lymphoma

Xinyi Tang[1], **Zhi-Zhang Yang**[1], **Hyo Jin Kim**[1], **Theodora Anagnostou**[1], **Yue Yu**[2], **Xiaosheng Wu**[1], **Jun Chen**[2], **Jordan E. Krull**[1], **Kerstin Wenzl**[1], **Patrizia Mondello**[1], **Vaishali Bhardwaj**[1], **Junwen Wang**[3], **Anne J. Novak**[1], **Stephen M. Ansell**[1]

[1]Division of Hematology and Internal Medicine, Mayo Clinic, Rochester, Minnesota.

[2]Department of Quantitative Health Sciences, Mayo Clinic, Rochester, Minnesota.

[3]Department of Quantitative Health Sciences and Center for Individualized Medicine, Mayo Clinic, Scottsdale, Arizona.

Abstract

Purpose: Regulatory T-cells (Treg) are essential to Tregs homeostasis and modulate the antitumor immune response in patients with lymphoma. However, the biology and prognostic impact of Tregs in splenic marginal zone lymphoma (SMZL) have not been studied.

Experimental Design: Biopsy specimens from 24 patients with SMZL and 12 reactive spleens (rSP) from individuals without lymphoma were analyzed by using CITE-seq (cellular indexing of transcriptomes and epitopes by sequencing), CyTOF (mass cytometry) analysis, and flow cytometry to explore the phenotype, transcriptomic profile, and clinical significance of intratumoral Tregs and their subsets. The biological characteristics and cell signaling pathways of intratumoral Treg subsets were confirmed by *in vitro* functional assays.

Results: We found that Tregs are more abundant in SMZL patients' spleens than rSP, and Tregs from patients with SMZL and rSP can be separated into CD161^{+}Treg and CD26^{+}Treg subsets. CD161^{+}Tregs are increased in SMZL but have dysregulated immune function. We found that CD161^{+}Treg and CD26^{+}Tregs have unique gene expression and phenotypic profiles and are differentially correlated with patient outcomes. Specifically, increased CD161^{+}Tregs are significantly associated with a favourable prognosis in patients with SMZL, whereas CD26^{+}Tregs

Corresponding Authors: Stephen M. Ansell, Division of Hematology, Mayo Clinic, 200 First Street SW, Rochester, MN 55905. ansell.stephen@mayo.edu; and Zhi-Zhang Yang, yang.zhizhang@mayo.edu.

Authors' Contributions

X. Tang: Data curation, software, formal analysis, funding acquisition, investigation, methodology, writing–original draft, project administration, writing–review and editing. **Z.-Z. Yang:** Data curation, formal analysis, supervision, methodology, writing–original draft, project administration, writing–review and editing. **H.J. Kim:** Data curation, methodology. **T. Anagnostou:** Resources, data curation, investigation, methodology. **Y. Yu:** Data curation, software, formal analysis, investigation, methodology, writing–review and editing. **X. Wu:** Resources, data curation, methodology, writing–review and editing. **J. Chen:** Data curation, software, formal analysis, writing–review and editing. **J.E. Krull:** Data curation, software, writing–review and editing. **K. Wenzl:** Data curation, software. **P. Mondello:** Validation, writing–review and editing. **V. Bhardwaj:** Validation. **J. Wang:** Software. **A.J. Novak:** Methodology, writing–review and editing. **S.M. Ansell:** Conceptualization, data curation, supervision, funding acquisition, investigation, writing–original draft, project administration, writing–review and editing.

The costs of publication of this article were defrayed in part by the payment of page charges. This article must therefore be hereby marked *advertisement* in accordance with 18 U.S.C. Section 1734 solely to indicate this fact.

Supplementary data for this article are available at Clinical Cancer Research Online (http://clincancerres.aacrjournals.org/).

are associated with a poor prognosis. Furthermore, activation of the IL2/STAT5 pathway contributes to the induction of $CD26^+$Tregs and can be reversed by STAT5 inhibition.

Conclusions: IL2/STAT5-mediated expansion of $CD26^+$Tregs contributes to a poor clinical outcome in SMZL and may represent a therapeutic opportunity in this disease.

Introduction

Splenic marginal zone lymphoma (SMZL) is an indolent B-cell non-Hodgkin lymphoma (NHL), involving lymphocytes of the splenic marginal zone and affecting the spleen, bone marrow, and peripheral blood (1). Although malignant B cells predominate in the tumor microenvironment, immune cells, including T cells, are frequently present and are assumed to be targeting the malignant clone (2, 3). However, it is assumed that the antitumor immune response is ineffective and the disease progresses over time. It has also been acknowledged that the immune microenvironment plays an indispensable role in determining both the natural history of lymphoma and the responsiveness to therapy (4–7). Although many patients with varied tumor types have benefited from immunotherapeutic interventions including checkpoint blockade (8–12) to activate T cells that are targeting the malignant clone, most patients with NHL have experienced modest or no clinical response when provided the same treatment (13). Patients with indolent B-cell NHL particularly have a very low overall response rate when treated with nivolumab (14). Therefore, additional studies on the diversity of the tumor immune microenvironment in B-cell NHL, and the function of intratumoral T cells, have profound implications for future immunologic treatment of indolent lymphomas including SMZL.

It is well known that immunosuppression plays an important role in the severity of cancer and the responsiveness to therapy. Regulatory T cells (Treg) are a specialized subpopulation of T cells, which can suppress the activation of other immune cells (15, 16). In some solid tumors and hematologic malignancies, including some lymphomas, high numbers of Tregs are associated with a poor prognosis due to the suppression of antitumor immune response (17–19). Also, degranulation and subsequent cytotoxic activity of infiltrating $CD8^+$T cells exposed to lymphoma B cells are attenuated by the presence of intratumoral Tregs (20). Nevertheless, several studies have shown that increased numbers of intratumoral Tregs are associated with improved overall survival in NHL, suggesting that Tregs may have a role in directly regulating malignant lymphoma cells (21–23). As the function of Tregs in SMZL is largely unknown, additional studies exploring the impact of Tregs on the antitumor immune response in this disease are clearly needed. Specifically, an in-depth investigation of the complexity and diversity of Tregs in SMZL is required to clarify their role as potential prognostic and therapeutic biomarkers in an otherwise favorable disease. In this study, we first assessed the abundance of Tregs in splenectomy specimens from patients with SMZL compared with nonlymphoma controls. Using CITE-seq, we then investigated the transcriptomic and phenotypic profiles of Treg subsets in the tumor microenvironment of patients with SMZL compared with controls and identified two differently expressed Treg subsets, which were characterized by either CD161 or CD26 surface expression. We further dissected their phenotype, function, and clinical relevance and identified the putative mechanisms promoting the prevalence of these Treg subsets in SMZL.

Materials and Methods

Patient samples

Patients providing written informed consent were eligible for this study if they had a tissue biopsy that on pathologic review showed splenic marginal zone lymphoma (SMZL) and adequate tissue to perform the experiments. Peripheral blood mononuclear cells (PBMCs) from healthy donors as well as spleens from patients with splenic hyperplasia without lymphoma were used as controls. Histologic diagnosis was performed according to World Health Organization criteria by an expert pathologist. The study was approved by the Institutional Review Board of the Mayo Clinic/Mayo Foundation. The study was conducted in accordance with the Declaration of Helsinki. Patient characteristics are summarized in Supplementary Table S1. Patients did not receive any therapy before undergoing a splenectomy.

Cell isolation and purification

Spleen tissue biopsy specimens from patients with SMZL and reactive spleen (rSP) were gently minced over a wire mesh screen to obtain a cell suspension. The cell suspension or peripheral blood from patients or healthy donors was centrifuged over Ficoll Hypaque at 1,200 rpm for 20 minutes to isolate mononuclear cells. $CD3^+$T and $CD8^+$T cells were isolated using negative selection with Human T-cell Enrichment Kit and Human $CD8^+$T cell enrichment Kit, respectively (StemCell Technologies). Regulatory T-cell subsets ($CD4^+CD25^+CD127^{low}$) were isolated using a flow sorter after being stained with the following fluorochrome-conjugated antibodies: antihumanCD4-FITC (BD Bioscience), anti-humanCD25-PE-Cy7 (BD Bioscience), anti-humanCD127-BV421 (BD Bioscience).

Mass cytometry (CyTOF) assay

CyTOF assay was performed according to the manufacturer's instructions as described previously (24). Briefly, three million cells were stained with 5 μmol/L Cell-ID Cisplatin (Fluidigm) for 5 minutes and quenched with MaxPal Cell Staining Buffer (Fluidigm). After centrifugation, cell suspensions (50 μL) were incubated with 5 μL of human Fc-receptor Blocking solution (BioLegend) for 10 minutes and 50 μL of premixed antibody cocktail (Supplementary Table S2) for 30 minutes. After washing, cells were incubated with 1 mL of cell intercalation solution (125 nmol/L MaxPal Intercalator-Ir into 1 mL MaxPal Fix and Pem Buffer) overnight at 4°C. Cells were centrifuged with MaxPal Water and pelleted. The pelleted cells were suspended with EQ Calibration Beads (Fluidigm) and cell events were acquired by a CyTOF II instrument (Fluidigm).

CyTOF data analysis

All samples were normalized and analyzed simultaneously to account for variability in signal across acquisition time. A high-level gating strategy was applied simultaneously to all CyTOF files (Supplementary Fig. S1). For specific analysis purposes, we isolated Tregs events (Tregs: $CD45^+CD3^+CD19^-$ $CD4^+CD8^-CD25^+CD127^{low}$) in each sample, saved them as individual sample Tregs files, and concatenated them. A tSNE map was generated by t-Distribution Stochastic Neighbor Embedding (tSNE) analysis to

make pairwise comparisons of cellular phenotypes, to optimally plot similar cells close to each other and to reduce multiple parameters into two dimensions (tSNE1 and tSNE2). Equal events per sample were selected for most analyses. Channel selection depended on cell populations to be clustered. Standard tSNE parameters (3,000 iterations, perplexity of 30 and θ of 0.5) were used. For identification of Tregs phenotype based on surface marker staining the following channels were selected: CD161, CD26,CCR6,PD-1,BTLA(CD272),CD7,CD69,TIM-3,ICOS,CD28, HLA-DR, CD45RA, TIGIT, CD141, KLRG1, CD57, CXCR1, CCR5, CXCR3, CD5, CD27, LAG-3, CD127(IL-7R), CD25(IL-2R), 4–1BB (CD137), CCR4, CCR7. Heatmaps were generated using Cytobank software (25). A color palette is included in the figures below the heatmaps.

CITE-seq assay

CITE-seq assay was performed according to the manufacturer's instructions as described previously (26). $CD3^{+}$T cells (1×10^{6}) were resuspended in 50 μL staining buffer and incubated for 10 minutes with an Fc receptor blocker (Human TruStain FcX; BioLegend). Subsequently, cells were incubated with mixtures of TotalSeq-C antibodies (Supplementary Table S3) for 30 minutes at 4°C. Cells were washed three times in cell staining buffer, followed by centrifugation (350 g 5 minutes at 4°C). After the final wash, cells were resuspended at appropriate cell concentrations (700–1,200 cells/μL, viability >90%) in calcium and magnesium-free 1 × PBS (Corning) containing 0.04% BSA (Thermo Fisher Scientific) and run by 10x Genomics applications. The cells were first counted and measured for viability using the Vi-Cell XR Cell Viability Analyzer (Beckman-Coulter). The barcoded Gel Beads were thawed from −80°C and the cDNA master mix was prepared according to the manufacturer's instructions for Chromium Single Cell 5′ Library and Gel Bead Kit (10× Genomics). On the basis of the desired number of cells to be captured for each sample, a volume of live cells was mixed with the cDNA master mix. The cell suspension and master mix, thawed Gel Beads and partitioning oil were added to a Chromium Single Cell A chip. The filled chip was loaded into the Chromium Controller, where each sample was processed and the individual cells within the sample were partitioned into uniquely labeled GEMs (Gel Beads-In-Emulsion). The GEMs were collected from the chip and taken to the bench for reverse transcription, GEM dissolution, and cDNA clean-up. The full-length cDNA was amplified and separated by size selection. The resulting cDNA created a pool of uniquely barcoded molecules used to generate 5′ gene expression libraries (GEX). In addition, the supernatant from the cDNA clean-up step contained amplified DNA from cell surface protein feature barcodes. That DNA was further cleaned and used to create cell surface protein libraries. During library construction, standard Illumina sequencing primers and a unique i7 Sample index (10× Genomics) were added to each cDNA and DNA pool (creating gene expression and feature barcodes libraries, respectively). All cDNA and DNA pools and resulting libraries were measured using Qubit High Sensitivity assays (Thermo Fisher Scientific) and Agilent Bioanalyzer High Sensitivity chips (Agilent).

GEX were sequenced at a minimum of 50,000 fragment reads per cell and feature barcodes libraries were sequenced at 5,000 fragment reads per cell. Sequencing steps followed Illumina's standard protocol using the Illumina cBot and HiSeq 3000/4000 PE Cluster Kit.

For gene expression libraries, the flow cells were sequenced as 100×2 paired end reads on an Illumina HiSeq 4000 using HiSeq 3000/4000 Sequencing Kit and HCS v3.3.52 collection software. For feature barcodes libraries, the flow cells were sequenced as 100×2 paired end reads on an Illumina HiSeq 4000. Base-calling was performed using Illumina's RTA version 2.7.3.

CITE-seq analysis

Reads were aligned to the human reference sequence GRCh38 as described before (26). We used Cell Ranger multi-pipeline to analyze FASTQ data derived from Gene Expression data (GEX) that contains the sequence data from the clusters that pass filter on a flow cell and feature barcode (antibody) library from the same GEM Well. We used the Seurat package (v4.0.1) to perform integrated analyses of single cells (27). After selecting the $CD4^{+}$T cells based on their gene expression in each CITE-seq dataset (CD3E-GENE > 0, CD19-GENE = 0, CD4-GENE > 0, CD8A-GENE = 0, and CD79A-GENE = 0), we followed the Seurat integration workflow and the comparative analysis workflow. The datasets were integrated on the basis of "anchors" identified between datasets before principal component analysis (PCA) was performed to make the linear dimensional reduction, and the UMAP was generated to identify clusters. The FindNeighbors algorithm was run on the low-dimensional space [top 20 statistically significant, principal components (PC)]. The FindClusters algorithm was performed on default and selected a resolution of 0.6. Enriched marker genes and proteins in each cluster conserved across all samples were identified and differentially expressed genes between clusters were detected by using the default Wilcoxon Rank Sum test at the cluster level. The R code used to analyze CITE-seq data can be accessed from https://codeocean.com/capsule/7530644.

GSEA analysis

We implemented GSEA using the Cluster Profiler package in R to perform enrichment analysis of gene sets generated from CITE-seq (28). The Benjamini and Hochberg (BH) method adjusted P value < 0.05 was used as the cutoff to determine significance for enrichment score (29).

Flow cytometry and intracellular staining

For surface marker detection, 1×10^6 or 1 million cells were washed in PBS and incubated with fluorochrome-conjugated antibodies (Abs) against and analyzed on a flow cytometer: anti-humanCD4-FITC (BD Bioscience), anti-humanCD25- PE-Cy7 (BD Bioscience), anti-humanCD127- BV421 (BD Bioscience), anti-humanCD161-APC (BioLegend), anti-humanCD26-PerCP/Cyanine5.5 (BioLegend). For apoptosis detection, Treg subsets were cultured in 96-well plate at 37°C in the presence of 5% CO_2. After 72 hours, cells were stained with PI/annexin V-APC and analyzed by flow cytometry. For Ki67 expression detection, Treg subsets were cultured in 96-well plate at 37°C and 5% CO_2 in the presence of Dynabeads Human T-Activator CD3/CD28 (Gibco). After 72 hours, cells were fix and permeabilized with reagents from Fixation/Permeabilization Solution Kit (BD Bioscience). Cells were then stained with anti-humanKi67-BV421 (BD Horizon) and analyzed by flow cytometry. See Supplementary Tables S4 and S5 for details of the flow cytometry antibodies and other reagents used.

Stat5 phosphorylation assay

Phosphorylation of Stat5 was determined by using flow-based intracellular staining following the instructions described by the manufacturer (BD Biosciences). Briefly, freshly isolated of Treg subsets and T effector cells were incubated with IL2 (50 ng/mL) for 20 minutes in a 37°C water bath. Cells were subjected to fixation with Fixation buffer (BD Biosciences) and permeabilization with Perm Buffer III (BD Biosciences). Cells were then stained with anti-Stat5(pY694)-PE (BD Biosciences) and analyzed by flow cytometry. See Supplementary Tables S4 and S5 for details of the flow cytometry antibodies and other reagents used.

Tregs subset development detection

$CD161^+CD26^-$Tregs ($CD4^+CD25^+CD127lowCD161^+CD26^-$), $CD26^+CD161^-$Tregs ($CD4^+CD25^+CD127lowCD161^-CD26^+$), double-negative Tregs (DNTregs; $CD4^+CD25^+CD127lowCD161^-CD26^-$), $CD26^+$Tconv cells ($CD4^+CD25^-CD127^+$ $CD26^+$) and CD26-T conv cells ($CD4^+CD25^-CD127^+$ $CD26^-$) were sorted by flow cytometry. Subsequently, different Treg subsets were incubated with or without IL2 (50 ng/mL; R&D Systems) in 96-well plates at 37°C in the presence of 5% CO_2. Cells were stained with anti-humanCD161-APC (BioLegend), anti-humanCD26-PerCP/Cyanine5.5 (BioLegend) and anti-humanKi67-BV421(BD Horizon) and then analyzed on a flow cytometer. DN Tregs ($CD4^+CD25^+CD127lowCD161^-CD26^-$) were sorted by flow cytometry. Purified DN Tregs were incubated with or without IL2 in the present or absent of Dynabeads Human T-Activator CD3/CD28. STAT5 inhibitor-573108 (Millipore) was used to block STAT5 phosphorylation. See Supplementary Tables S4 and S5 for details of the flow cytometry antibodies and other reagents used.

CFSE labeling and Tregs suppression assay

$CD4^+CD25^-$T conventional cells $CD161^+CD26^-$Tregs ($CD4^+CD25^+CD127lowCD161^+CD26^-$) and $CD26^+CD161^-$Tregs ($CD4^+CD25^+CD127lowCD161^-CD26^+$) were sorted by flow cytometry. To determine their effect on T cells, $CD8^+$T were isolated from the PBMCs of healthy donors by using negative selection with the Human $CD8^+$T Cell Enrichment Kit (StemCell Technologies). A stock solution of CFSE (5 mmol/L; Invitrogen) was added to the $CD8^+$T cells or B cells for a final concentration of 5 μmol/L. After 15 minutes at 37°C, cells were washed three times with 10 volumes of RPMI1640 Media (Gibco) containing 5% FBS. CFSE-labeled $CD8^+$T cells (1×10^5) were cultured with $CD161^+CD26^-$Tregs (1×10^5) and $CD26^+CD161^-$Tregs (1×10^5) respectively with the presence of 2 μL Dynabeads human T-activator CD3/CD28 in 96-well plate at 37°C in the presence of 5% CO_2. Cells were harvested at day 3 and analysed on a flow cytometer. Proliferation of $CD8^+T_{CFSE}$ was evaluated by the CFSE dilution assay. Suppressive function was calculated [%Suppressive = 100 – (%proliferating cells with Tregs present/%proliferating cells without Tregs present) × 100; refs. 30, 31].

To determine the effect of Tregs on B cells, CFSE-labeled $CD19^+$B (1×10^5) cells were cultured with T conventional cells (1×10^5), $CD161^+CD26^-$Tregs (1×10^5), and $CD26^+CD161^-$Tregs (1×10^5) respectively with the presence of Functional Grade anti-CD3 (OKT3; 10 μg/mL) and anti-CD28 (2 μg/mL), CpG-B DNA (0.7 μmol/L; Hycultbiotech),

CD40 L (1 μg/mL; enzo lifesciences), and IL4 (50U/mL; Peprotech). Cells were harvested at day 3 and analyzed on a flow cytometer. Proliferation of B cells was evaluated by the percentage of $CFSE^{dim}$ and $Ki67^{+}$ B cells. See Supplementary Tables S4 and S5 for details of the flow cytometry antibodies and other reagents used.

Statistical analysis

Statistical analysis was performed in GraphPad Prism 8 and R (R version 4.0.3). Significance was determined at $P < 0.05$. For unpaired and normal distribution data, statistical analysis was performed using the two-tailed *t* test. For unpaired and variables without normal distribution, we used the nonparametric Mann–Whitney test. For matched-paired data, the paired *t* test or Wilcoxon matched-pairs signed rank test were used for data with or without a normal distribution, respectively. Event-free survival (EFS) was measured from the date of splenectomy until the date of relapse, progression, additional therapy, or death. All patients had a splenectomy at the time of diagnosis. Early failure was defined as failure to achieve EFS of 24 months after splenectomy (EFS24; ref. 32). EFS of all patients was estimated using the Kaplan–Meier method and compared by using Log-rank test. To associate the Treg subset with the patient outcomes, we combined data generated by CyTOF and flow cytometry. To adjust for the batch differences, we use a subset of samples measured by both CyTOF and flow cytometry as “bridge” samples and use the Location and scale (L/S) batch adjustment model to correct the batch differences. The location and scale (L/S) adjustment model can be defined as a wide family of adjustments in which one assumes a model for the location (mean) and scale (variance) of the data within batches and then adjusts the batches to have the same location and scale (33).

Data availability

The data generated in this study are available upon request from the corresponding author.

Results

Intratumoral Tregs are enriched in patients with SMZL

To explore the heterogeneity of Tregs in the tumor microenvironment of SMZL, we first measured the frequency of Tregs in 17 patients with SMZL using CyTOF. Six reactive spleens (rSP) from individuals without lymphoma were utilized as a control. The patient characteristics were summarized in Supplementary Table S1. Tregs were identified as $CD4^{+}CD25^{+}CD127^{low}$ cells using a gating strategy (Fig. 1A). To minimize the variance between samples, we first concatenated all data from $CD4^{+}$ cells from each SMZL or rSP sample into a single file, and then performed tSNE analysis to visualize the presence of Tregs. As shown in Fig. 1B, a cluster of cells that was $CD25^{+}$ and $CD127^{-}$ were presented in $CD4^{+}$T cells from both SMZL and rSP with the cluster size being larger in SMZL than rSP (13.03% vs. 4.24%), indicating an increased prevalence of Tregs in SMZL. Individual sample data of 17 SMZL and 6 rSP confirmed that the percentage of Tregs within $CD4^{+}$ compartment was significantly higher in spleens from patients with SMZL than that from rSP, also showed expected variability of Tregs among the cohort samples (Fig. 1C).

We next explored the phenotype of intratumoral Tregs in SMZL. $CD4^+CD25^+$ $CD127^-$ cells from 17 patients with SMZL were concatenated and analyzed using tSNE plots. As shown in Fig. 1D, the vast majority of Tregs lacked CD45RA expression, suggesting a memory phenotype for Tregs. Among these CD45RA-Tregs, a substantial number of cells expressed CCR7, suggesting a central memory type for some Tregs. One subset of Tregs expressed CD57, suggesting a terminally differentiated phenotype for this subset of Tregs. This confirmed the heterogeneity of intratumoral Tregs in SMZL and suggested that they may constitute distinct subsets with specific functions. Therefore, additional in-depth analysis of the genome and proteome of each subset was indicated.

Multi-omics analysis of $CD4^+$T cells identifies two Treg subsets in SMZL

To further understand intratumoral $CD4^+$T cells in SMZL, we performed single-cell CITE-seq analysis and profiled $CD4^+$T cells from three rSP and three patients with SMZL (Fig. 2A). Using the default clustering in Seurat, we identified eleven clusters, representing 11 subpopulations of intratumoral $CD4^+$T cells (Fig. 2B; Supplementary Fig. S2A). These subpopulations included memory cells (Tm), naïve cells (Tn), follicular helper T cells (Tfh), regulatory T cells (Treg) among others (Fig. 2B and C; Supplementary Fig. S2B). Transcripts of *FOXP3*, *IL2RA*, and *CTLA4* were abundantly expressed in cells from Cluster4 and Cluster9, identifying these as Treg clusters (Fig. 2C, left). Compared with Cluster4, the cells of Cluster9 showed expression of *KLRB1* (Fig. 2C, right and D), which encodes NK-cell-receptor protein 1A, also known as CD161. CD161 is a C-type lectin-like receptor mainly expressed on NK cells but may also be present on T cells, including $CD4^+$Tfh, $CD4^+$Tregs, and $CD8^+$T cells. We next compared differentially expressed genes between *KLRB1*-Tregs and *KLRB1*+Tregs in concatenated SMZL samples, and 428 genes were differentially expressed between these two Treg subsets (Fig. 2E; Supplementary Table S6). Among these genes, 29 genes were significantly higher and 98 genes significantly lower in *KLRB1*-Tregs compared with *KLRB1*+Tregs ($|\log_2 FC| > 0.5$, adjusted *P* value <0.05; Fig. 2E). In particular, *KLRB1*+Tregs had increased expression of *PDCD1*, *TNFRSF18*, *TNFRSF4*, and *CTLA4*, whereas *KLRB1*-Tregs expressed higher levels of *CCR4*, *CCR7*, *IL2RA*, and *FOXP3* (Fig. 2F). Moreover, we compared the gene expression profile of *KLRB1*+Tregs and *KLRB1*-Tregs in SMZL versus reactive spleens. As shown in Supplementary Fig. S2C(i) (Supplementary Table S7), there are 1,431 differentially expressed genes between *KLRB1*+Tregs from SMZL and rSP, of which 29 genes were statistically significantly different (adjusted *P*-value <0.05). Similarly, there were 670 differentially expressed genes between *KLRB1*-Tregs from SMZL and rSP, and 134 genes were statistically significantly different [adjusted *P* value <0.05; Supplementary Fig. S2C (ii); Supplementary Table S8]. Compared with *KLRB1*+Tregs in rSP, *KLRB1*+Tregs in SMZL had significantly higher *FOXP3* and lower ICOS expression. Compared with reactive spleen, KLRB1-Tregs in SMZL had higher *CISH*, *TNFRSF18* (GITR) and lower *TNFSF8* (CD153, CD30L) and *IL-7R* expression. In addition, both $KLRB1^+$Tregs and $KLRB1^-$Tregs derived from patients with SMZL had higher *IL32* expression than rSP.

Next, we validated single-cell signatures at the protein level and measured the expression profile of surface markers of *KLRB1*-Tregs (Cluster4) and $KLRB1^+$Tregs (Cluster9) using CITE-seq. In this cohort, we stained cells with 35 surface markers in CITE-seq assay

(Supplementary Table S3), and the combination of CD25 (IL2R-TotalSeqC) and *FOXP3* clearly delineated Tregs [Fig. 2G (i) and (ii)]. Compared with *KLRB1*$^{-}$Tregs, *KLRB1*$^{+}$Tregs showed a different expression profile of surface markers [Fig. 2G (iii)]. As expected, CD161, the protein encoded by the *KLRB1* gene, was highly expressed in *KLRB1*$^{+}$Tregs (Cluster9) and negative in *KLRB1*$^{-}$Tregs (Cluster4). In addition, *KLRB1*$^{+}$Tregs expressed higher levels of PD-1 and BTLA and less CCR4 and CCR7, which were highly expressed on the surface of *KLRB1*$^{-}$Tregs (Fig. 2H).

CD161 and CD26 expression defines Treg subsets

The identification of *KLRB1*$^{+}$ or *KLRB1*$^{-}$Tregs with CITE-seq led us to further evaluate these Tregs in patients with SMZL. Using CyTOF, we found that CD161 protein encoded by *KLRB1* gene and CD26 were reciprocally expressed on CD4^{+}CD25^{+}CD127^{low}Tregs, forming two subsets of Tregs: CD161^{+} and CD26^{+}Tregs (Fig. 3A). These two subsets exhibited different phenotypes (Fig. 3B). Surface markers that were upregulated in one subset were downregulated in the other subset and vice versa. Expression of PD-1, BTLA, and ICOS were upregulated in CD161^{+}Tregs when compared with CD26^{+}Tregs. In contrast, CD26^{+}Tregs expressed increased CD25, 4–1BB, CCR4, and CCR7 compared with CD161^{+}Tregs (Fig. 3B). The results from 17 patient samples are summarized in Fig. 3C, indicating that both the percentage and median marker intensity of each marker were significantly higher in one subset than the other. The expression of other surface markers is presented in Supplementary Figs. S3A and S3B.

CD161^{+} and CD26^{+}Tregs exhibit differing capacities for cell proliferation, survival, and immune suppression

Given the different phenotypes of these two Treg subsets, we posited that CD161^{+} and CD26^{+}Treg subsets were functionally different as well. To test this hypothesis, we assessed the proliferative capacity of these two subsets using sorted CD161^{+} and CD26^{+}Tregs from PBMCs of healthy donors. We cultured both T-cell subsets using a Dynabeads Human T-Activator assay (Supplementary Fig. S4A). After 3 days, the percentage of Ki67^{+} cells were evaluated. Compared with CD161^{+}Tregs, the Ki67^{+} population in the CD26^{+}Treg fraction was significantly increased, suggesting CD26^{+}Tregs exhibit superior proliferative ability compared with CD161^{+}Tregs (Fig. 4A). Given the increased expression level of exhaustion makers, including PD-1 and BTLA, on CD161^{+}Tregs, we wondered whether the survival of these two subsets could differ. Using annexin V (AnV) and propidium iodide (PI) staining, we observed that the CD161^{+}Tregs had decreased viability compared with CD26^{+}Tregs after 72 hours in culture as the number of live cells (AnV^{-}PI^{-}) was significantly lower in CD161^{+}Tregs than CD26^{+}Tregs. In contrast, the number of early apoptotic (AnV^{+}PI^{-}) and late apoptotic/necrotic (AnV^{+}PI^{+}) cells was significantly higher in CD161^{+}Treg than CD26^{+}Tregs (Fig. 4B). These results indicate that CD161^{+}Treg subsets are highly susceptible to apoptosis.

We next explore the immune suppressive function of these two Treg subsets. In the presence of Human T-Activator Dynabeads, CD161^{+}Treg or CD26^{+}Tregs were co-cultured with CFSE-labeled CD8^{+}T cells (Responding T cells, Tresp) at different ratios (Treg subsets: Tresp = 1:1–8; Supplementary Fig. S4B; Fig. 4C). In the absence of Tregs, a majority of

CD8$^+$T cells proliferated in response to activation. CD161$^+$Tregs exhibited a dose-dependent inhibition of CD8$^+$T cell proliferation as the number of CD8$^+$ CFSE^{dim} cells increased when the Treg:Tresp ratio decreased. In contrast, this inhibitory effect was weak when CD8$^+$T cells were cocultured with CD26$^+$Tregs. The number of CD8$^+$ CFSE^{dim} cells stayed stable when the number of Tregs increased (Fig. 4C). We calculated the suppression index using a formula (shown in the Materials and Methods). As shown in Fig. 4D, CD161$^+$Tregs showed significantly greater suppression of CD8$^+$T cell proliferation than CD26$^+$Tregs.

In addition to suppression of CD8$^+$T cells, we also investigated the immunosuppressive effect of CD161$^+$ and CD26$^+$Tregs on normal and malignant B cells. To do this, CFSE labeled B cells were cocultured with CD161$^+$Tregs, CD26$^+$Tregs, or CD4$^+$CD25$^-$CD127^{high}T (conventional T cell, Tconv) from PBMCs of healthy donors in thepresence of IL4 and CD40L. After 3 days, the proliferation of B cells was evaluated by measuring thenumber of divided B cells(CFSE^{dim}Ki67$^+$), undivided B cells (CFSE$^+$Ki67$^-$), CFSE^{dim}B cells and Ki67$^+$B cells (Fig. 4E). As shown in Fig. 4F and G, compared with B cells cocultured with CD26$^+$Tregs and conventional T cells, the number of divided B cells (i), CFSE^{dim} cells (iii), and Ki67$^+$ cells (iv) co-cultured with CD161$^+$Tregs was significantly decreased. When malignant B cells from patients with SMZL were used in the assay, the frequency of viable or Ki67$^+$B cells cocultured with CD161$^+$Tregs were lower than when cocultured with CD26$^+$Tregs or Tconv (Fig. 4H and I). In addition, when B cells from lymph nodes were cocultured with Treg subsets, the frequency of viable and Ki67$^+$B cells cocultured with CD161$^+$Tregs were lower than when cocultured with CD26$^+$Tregs or Tconv (Supplementary Figs. S4C and S4D). Taken together, these results suggest that CD161$^+$Tregs are more immunosuppressive, but more prone to apoptosis and less proliferative when compared with CD26$^+$Tregs.

IL2 promotes the development of CD26$^+$Tregs with the involvement of STAT5

Next, we explored the signaling pathways activated in the various Treg subsets. Gene set enrichment analysis (GSEA) of differentially expressed genes between intratumoral SMZL CD26$^+$ and CD161$^+$Tregs was performed from CITE-seq data. Figure 5A shows the top five enriched pathways in either CD26$^+$ or CD161$^+$Tregs. Among the identified pathways, the inflammatory response and IL2/STAT5 pathways were significantly upregulated in CD26$^+$Tregs compared with CD161$^+$Tregs [Fig. 5B(i)]. Consistent with the pathway analysis, we found that after treatment of total Tregs with IL2 for 72 hours, the percentage of CD26$^+$Tregs increased, but the frequency of CD161$^+$Tregs did not change (Supplementary Fig. S5A). We hypothesized that IL2 preferentially enhances the proliferation of CD26$^+$Tregs or may promote the expression of CD26 on Tregs. This was in line with the findings that the expression of IL2RA mRNA was significantly higher in CD26$^+$Tregs than that in CD161$^+$Tregs [Fig. 5B(ii)], and that CD26$^+$Tregs showed higher CD25 expression level (Fig. 3C). To further explore the role of IL2 in the development of Treg subsets, we isolated and treated CD161$^+$, CD26$^+$, and DN Tregs, with IL2 for 72 hours. After treatment, the expression of Ki67 as well as CD26 and CD161 was measured to evaluate the development of Treg subsets. As shown in Fig. 5C, after IL2 treatment, the expression of CD26 was enhanced on CD161$^+$Tregs, CD26$^+$Tregs, and DN Tregs [Fig. 5C(iii)], whereas CD161 [Fig. 5C(ii)] and Ki67 [Fig. 5C(i)] expression was not changed by

IL2 treatment on each Treg subset. We next assessed the effect of IL2 on CD26 expression in Tconv cells. We sorted CD4$^+$T conventional cells from PBMCs of three healthy donors and then divided Tconv cells into CD26$^+$Tconv and CD26Tconv cells. After being treated with IL2, the expression of CD26 was upregulated on the surface of CD26-Tconv and slightly further upregulated on the surface of CD26$^+$Tconv (Supplementary Figs. S5B and S5C). These findings suggest that IL2 enhances CD26 expression on Tregs instead of promoting the proliferation of CD26$^+$Tregs. In other words, IL2 could skew Tregs toward a CD26$^+$Treg phenotype. STAT5 is a crucial target downstream of JAK kinases associated with IL2R, and the IL2–STAT5 pathway is significantly increased in CD26$^+$Tregs compared with CD161$^+$Tregs. Therefore, we detected the STAT5-Tyr694 phosphorylation level in CD161$^+$Tregs and CD26$^+$Tregs with or without IL2 treatment. As shown in Fig. 5D, compared with CD161$^+$Tregs, CD26$^+$Tregs have higher STAT5 phosphorylation levels with and without IL2 treatment. We then explored whether blocking STAT5 signaling with a STAT5 inhibitor affects the enhancement of CD26 expression mediated by IL2 on Tregs. As shown in Fig. 5E and F, DN Tregs (CD161$^-$CD26$^-$) treated with STAT5 inhibitor resulted in a downregulation of IL2-induced CD26 enhancement in resting and activated Tregs. Also, the activation of Tregs by anti-CD3 and anti-CD28 antibodies very modestly changed the expression of CD26 on Tregs, suggesting CD26 is not simply an activation marker but rather is upregulated by IL2 signaling with the involvement of STAT5.

Intratumoral CD161$^+$Tregs and CD26$^+$Tregs differentially correlate with patient outcomes in MZL

Next, we tested whether these Treg subsets in the tumor microenvironment were associated with patient outcomes in SMZL. We compared the percentage of Tregs in CD4$^+$T cells from patients with SMZL (n = 24) with those from rSP from patients who did not have lymphoma (n = 12). As shown in Fig. 6A(i), the percentage of total Tregs in CD4$^+$T cells were significantly higher in patients with SMZL (SMZL median: 16.34%; rSP median: 11.33%; P = 0.006).

EFS24 is an important indicator of patient prognosis in lymphoma (32). We compared the prevalence of CD161$^+$Tregs and CD26$^+$Tregs in biopsy specimens from 24 previously untreated patients with SMZL who had long-term follow up (Supplementary Table S1). We grouped patients into those who achieved or failed EFS24. Although there was no difference in the frequency of total Tregs between patients who achieved or failed EFS24 [EFS achieved—median frequency of Tregs: 15.53%, EFS failed—median: 17.67%, P = 0.87; Fig. 6A(ii)], we found a significant difference in Treg subsets in these groups (Fig. 6B). Specifically, patients who achieved EFS24 had significantly increased numbers of CD161$^+$Tregs (EFS achieved—median: 36.31%; EFS failed—median: 13.60%; P = 0.007) and decreased CD26$^+$Tregs (EFS achieved—median: 17.03%; EFS failed—median: 43.44%; P = 0.004), respectively [Fig. 6C(i) and (ii)]. To investigate whether age differences lead to variance in Treg cell subsets, we compared the frequencies of total Tregs and Treg subsets in patients over and under 70 years of age. There were no differences in total Tregs and Treg subsets in patients over 70 years old compared with patients under 70 (Supplementary Fig. S6A). We then determined whether the frequency of total Treg cells, CD161$^+$ or CD26$^+$Treg cells correlated with event-free (EFS) in patients with SMZL. Although the frequency of

total Treg cells did not show a correlation with EFS [Fig. 6D(i)], an increased percentage of CD161^{+}Treg cells was significantly associated with a favorable EFS in this MZL patient cohort [$P = 0.0334$, Fig. 6D(ii)] using the median number of cells as a cutoff. In contrast, the percentage of CD26^{+}Treg cells showed a trend toward a poor EFS in patients with MZL, but the difference was not statistically significant [$P = 0.1234$, Fig. 6D(iii)]. In addition, we compared the ratio of CD8^{+}T cells to Tregs between patients who achieved EFS24 and those who failed to achieve this clinical milestone. We found patients who did not achieve EFS24 had a significantly higher CD8/Tregs ratio (Supplementary Fig. S6B).

Discussion

It has been shown that immune suppression plays a central role in immune homeostasis that affects the severity of cancer and the responsiveness to therapy (15, 16). Although Tregs are responsible in part for this suppression, the exact subtype of Tregs and role they play in lymphomas is understudied. Furthermore, the role that Tregs play in SMZL is unknown.

Tregs are a unique subset of CD4^{+}T cells that inhibit the activation of other immune cells and play a vital role in regulating tumor immunity. Clinically, the role of Tregs in predicting outcome in lymphoma is controversial. Although some studies have observed that high numbers of Tregs are associated with a poor prognosis due to the capacity of Tregs to diminish antitumor immune responses, other studies found that increased numbers and follicular localization of FOXP3 positive Tregs are associated with an improved favorable overall survival (17, 18, 21–23). These clinical observations suggest, in addition to mediating tumor immune escape by suppressing the immune system, Tregs may have a direct effect on B-cell neoplasms.

Our previous work has shown that Tregs are enriched in the tumor sites of B-cell NHL and significantly inhibit the function of autologous infiltrating CD4^{+}CD25^{-}T cells and CD8^{+}CTL cells (19, 20). In this study, specifically focused on SMZL, we found a significant enrichment of Tregs in biopsies from patients with SMZL compared with rSP. CyTOF analysis revealed that intratumoral Tregs are phenotypically heterogeneous. The majority of intratumoral Tregs lacked CD45RA expression, suggesting a memory phenotype for Tregs. These memory-like Tregs partially expressed CCR7, suggesting a central memory phenotype. One of our previous studies demonstrated that lack of intrafollicular central memory CD4+ expression was strongly associated with failing to achieve EFS12/24 in follicular lymphoma patients who received or did not immunochemotherapy. This implies that Tregs with similar phenotypes may also have prognostic value (34). In addition to the abundant expression of CD69, CD28, CD27, and CD7, the intratumoral Tregs partially express PD-1. These PD-1 positive Tregs also expressed ICOS, BTLA, and TIGIT. Furthermore, CD161 and CD26 were mutually-exclusively expressed on Tregs.

To better understand the heterogeneity and the transcriptome of intratumoral Tregs in patients with SMZL, we performed CITE-seq to profile CD4^{+}T cells from 3 rSP individuals and 3 patients with SMZL. As a result, we identified two subsets of intratumoral Tregs. These two subsets of Tregs have different transcriptomes and surface marker profiles: one subset showed increased genetic expression of *KLRB1*, and another was negative for

KLRB1. *KLRB1* encodes NK-cell-receptor protein 1A, also known as CD161. CD161 is a C-type lectin-like receptor that is mainly expressed on the NK cells and has subsequently been identified on subsets of T cells, including $CD4^+$helper T cells, $CD4^+$regulatory T cells, and $CD8^+$T cells. Pesenacker and colleagues found a similar Treg subset in health and autoimmune diseases, which is also CD161 positive, displays high proinflammatory potential, but also exhibits typical Treg characteristics (35). In addition to this, Povoleri and his colleagues found that $CD161^+$Tregs are a highly suppressive, distinct subset of induced Tregs and can accelerate the wound healing of the colorectal epithelium (36). In this study, we found these CD161 positive and negative Treg subpopulations to be present in patients with SMZL.

Using CITE-seq and CyTOF, we found that, compared with $CD26^+$Tregs, $CD161^+$Tregs have significantly higher gene expression levels of *PDCD1*, *TNFRSF18*, *TNFRSF4*, and *CTLA4*, whereas $CD26^+$Tregs expressed higher levels of *CCR4*, *CCR7*, *IL2RA*, and *FOXP3*. For the surface markers, $CD161^+$Tregs express significantly higher levels of PD-1, BTLA, and ICOS. In contrast, $CD26^+$Tregs express higher levels of CD25, 4–1BB, CCR4, and CCR7. Compared with reactive spleen, $CD26^+$ (*KLRB1*-Tregs) Tregs in SMZL samples had higher *CISH*, *TNFRSF18* (GITR) and lower *TNFSF8* (CD153, CD30L) and *IL-7R* expression. In contrast, $CD161^+$Tregs (*KLRB1*+Tregs) in SMZL samples had higher *FOXP3* and lower *ICOS* expression. Each of these is a regulator of immune function. *CISH* is a negative regulator of TCR pathway (37), whereas *TNFRSF18* (GITR) is an immune checkpoint that is constitutively expressed in Treg cells (38). *TNFSF8* (encoding CD153, also known as CD30L) is expressed on the cell surface of activated T cells, and CD30/CD30L interactions induce T-cell apoptosis, preventing autoimmunity (39). In addition, both $CD26^+$Tregs and $CD161^+$Tregs derived from patients with SMZL have higher *IL32* expression than rSP. According to a recent study, knocking down of IL32 reduced Foxp3 expression in $CD4^+$T cells (40). In comparison to rSP, both $CD26^+$Tregs and $CD161^+$Tregs in patient with SMZL samples had higher expression of Treg signature genes.

These different phenotypes of $CD161^+$Tregs and $CD26^+$Tregs are functionally different as well. Our data indicated that $CD161^+$Tregs showed less viability and are more susceptible to apoptosis than $CD26^+$Tregs. For immunosuppressive function, $CD161^+$Treg showed significantly greater suppressive ability on $CD8^+$T cells than $CD26^+$Tregs. Of note, the immunosuppressive function of $CD161^+$Tregs on B cells is more robust than that of $CD26^+$Tregs. These suggest that Tregs may gain more ability to suppress malignant B cells when they are skewed towards a $CD161^+$ phenotype. Therefore, patients with more $CD161^+$Tregs may have a better prognosis due to suppression of the malignant B-cell clone. In contrast, Tregs have a less ability to inhibit B cells when they are skewed toward $CD26^+$Tregs, and more $CD26^+$Tregs in patients with SMZL may result in a worse disease outcome. In addition to suppressive function, $CD161^+FoxP3^+$T cells may display high proinflammatory potential (35). The plasticity between Treg and T helper type 17 (T_H17) may provide an explanation for this finding (41, 42). To evaluate the differences in signaling pathways that account forthese two subsets, we performed GSEA and found that the IL2–STAT5 pathway is significantly upregulated in $CD26^+$Tregs. Furthermore, the gene and protein levels of IL2RA are significantly higher in $CD26^+$Tregs than $CD161^+$Tregs. In addition, the phosphorylation level of STAT5-Try694 induced by IL2 is higher in

CD26^{+}Tregs than CD161^{+}Tregs and the upregulation of CD26 expression could be reversed by interrupting STAT5 signaling using an inhibitor that selectively targets the SH2 domain of STAT5 and blocks DNA binding activity (43). Moreover, the upregulation of CD26 expression is greater in activated Tregs because of increased expression of IL2R after TCR activation. However, we found the TCR activation alone did not increase the expression of CD26, suggesting CD26 is not simply an activation marker for Tregs. Also, STAT5 inhibition did not change the expression of CD26 in activated Tregs without the presence of IL2, confirming that IL2 signaling is needed for CD26 upregulation.

Although not specifically studied in SMZL, IL2 signaling has been shown to be relevant in other lymphomas. In previous studies, low serum IL2R levels were significantly associated with a favorable prognosis in Hodgkin lymphoma, and elevated sIL2Rα levels before treatment were associated with a poor outcome in patients with follicular lymphoma (44, 45). In previous work, we also found that IL2R binds and forms a complex with IL2 to prolong IL2 signaling, thereby promoting Treg function (46, 47). This indicates that IL2 signaling thatpromotes Treg formation is highly activated in lymphoid malignancies and is associated with poor prognosis in patients with lymphoma. Furthermore, we find that CD161^{+}Tregs have higher expression levels of several TNF and TNF receptor super family-related molecules, including TNFRSF18 and TNFRSF4. Interestingly, it has been reported that exogenous TNFα facilitates iTreg differentiation and function *in vitro* (48). We therefore hypothesize that the TNFa pathway is an additional pathway that promotes the expansion of CD161^{+}Tregs in patients with SMZL.

Taken together, these findings confirm that the IL2/STAT5-mediated signaling pathway promotes the development of CD26^{+}Tregs and skews Treg cell development away from CD161^{+}Tregs. This upregulated IL2/STAT5 signaling results in an unfavorable disease prognosis in patients with SMZL. In contrast, patients with SMZL who have a favorable outcome and who achieved EFS24 are those who have an increased number of CD161^{+}Tregs and a decreased number of CD26^{+}Tregs. Bonfiglio and colleagues have shown that patients with SMZL with an “immune-suppressive” microenvironment, with greater numbers of CD3^{+}T, CD4^{+}T, CD8^{+}T, and FOXP3^{+}T cells, have poorer 10-year survival rates. We find that the CD26^{+}Treg subgroup in our manuscript also has greater numbers of CD8^{+}T and FOXP3^{+}T cells. Although our analysis could not be perfectly correlated with the immune subtypes described in this reference, it may be that the CD26^{+}Treg subset in our study correlates best with the immune-suppressive subset described by Bonfiglio and colleagues (1).

In summary, high-dimensional and multi-omics single-cell analysis of the SMZL TME provides novel insights into the subtypes of intratumoral Tregs, which have not been previously studied in this malignancy. By comparing the intratumoral Treg subsets defined by CD161 and CD26 expression, we observed that the intratumoral Tregs from patients with SMZL who have a favorable clinical outcome are enriched for Tregs with a CD161-positive phenotype. It is acknowledged that this was demonstrated in a small SMZL cohort and further in-depth validation in a larger cohort is needed in the future. However, we also found that IL2/STAT5 signaling skews Tregs away from CD161^{+}Tregs that are associated with a favorable prognosis toward a CD26-positive phenotype that is associated with a poor

prognosis. Modulating the balance of Treg subsets by inhibiting IL2/STAT5 signaling and promoting the CD161^{+}Treg phenotype may therefore have substantial therapeutical potential and may improve the clinical outcome of patients with SMZL.

Supplementary Material

Refer to Web version on PubMed Central for supplementary material.

Acknowledgments

This work was supported by grants from the Department of Defense (W81XWH1810650), the Mayo Clinic/Iowa Lymphoma SPORE (P50 CA97274), a SEAFAM Discovery Grant from the Immuno-Oncology Program at Mayo Clinic (91314143), a CCatTS-CBD Pilot Award for Team Science (FP00120421), and the Predolin Foundation (91314145), National Library of Medicine (1R01LM013438). We thank Fariborz Rakhshan Rohakhtar, MS; Vernadette Simon, MS; and other colleagues in Mayo Clinic Medical Genome Facility Genome Analysis Core for performing the CITE-seq assay. We thank Ying Li, PhD, and other colleagues in Mayo Clinic Department of Quantitative Health Sciences for CITE-seq data primary analysis. We appreciate the Mayo Immune Monitoring Core for the assistance with the CyTOF analysis.

Authors' Disclosures

X. Wu reports grants from NCI outside the submitted work. A.J. Novak reports other support from Bristol Myers Squibb outside the submitted work. S.M. Ansell reports grants from Bristol Myers Squibb, ADC Therapeutics, Pfizer, Affimed, and Regeneron outside the submitted work. No disclosures were reported by the other authors.

References

1. Bonfiglio F, Bruscaggin A, Guidetti F, Terzi di Bergamo L, Faderl M, Spina V, et al. Genetic and phenotypic attributes of splenic marginal zone lymphoma. Blood 2022;139:732–47. [PubMed: 34653238]
2. Kahl B, Yang D. Marginal zone lymphomas: management of nodal, splenic, and MALT NHL. Hematology Am Soc Hematol Educ Program 2008:359–64. [PubMed: 19074110]
3. Bertoni F, Rossi D, Zucca E. Recent advances in understanding the biology of marginal zone lymphoma. F1000Res 2018;7:406. [PubMed: 29657712]
4. Hanahan D, Weinberg RA. Hallmarks of cancer: the next generation. Cell 2011; 144:646–74. [PubMed: 21376230]
5. Tarte K Role of the microenvironment across histological subtypes of NHL. Hematology Am Soc Hematol Educ Program 2017;2017:610–7. [PubMed: 29222311]
6. Vardhana S, Younes A. The immune microenvironment in Hodgkin lymphoma: T cells, B cells, and immune checkpoints. Haematologica 2016;101:794–802. [PubMed: 27365459]
7. Binnewies M, Roberts EW, Kersten K, Chan V, Fearon DF, Merad M, et al. Understanding the tumor immune microenvironment (TIME) for effective therapy. Nat Med 2018;24:541–50. [PubMed: 29686425]
8. Ansell SM, Lesokhin AM, Borrello I, Halwani A, Scott EC, Gutierrez M, et al. PD-1 blockade with nivolumab in relapsed or refractory Hodgkin's lymphoma. N Engl J Med 2015;372:311–9. [PubMed: 25482239]
9. Rizvi NA, Mazieres J, Planchard D, Stinchcombe TE, Dy GK, Antonia SJ, et al. Activity and safety of nivolumab, an anti-PD-1 immune checkpoint inhibitor, for patients with advanced, refractory squamous non-small-cell lung cancer (CheckMate 063): a phase 2, single-arm trial. Lancet Oncol 2015;16: 257–65. [PubMed: 25704439]
10. Gandhi L, Rodríguez-Abreu D, Gadgeel S, Esteban E, Felip E, De Angelis F, et al. Pembrolizumab plus Chemotherapy in metastatic non-small-cell lung cancer. N Engl J Med 2018;378:2078–92. [PubMed: 29658856]

11. Schmid P, Adams S, Rugo HS, Schneeweiss A, Barrios CH, Iwata H, et al. Atezolizumab and Nab-Paclitaxel in advanced triple-negative breast cancer. N Engl J Med 2018;379:2108–21. [PubMed: 30345906]
12. Forde PM, Chaft JE, Pardoll DM. Neoadjuvant PD-1 blockade in resectable lung cancer. N Engl J Med 2018;379:e14.
13. Ansell SM, Minnema MC, Johnson P, Timmerman JM, Armand P, Shipp MA, et al. Nivolumab for relapsed/refractory diffuse large B-cell lymphoma in patients ineligible for or having failed autologous transplantation: a single-arm, phase II study. J Clin Oncol 2019;37:481–9. [PubMed: 30620669]
14. Armand P, Janssens A, Gritti G, Radford J, Timmerman J, Pinto A, et al. Efficacy and safety results from CheckMate 140, a phase 2 study of nivolumab for relapsed/refractory follicular lymphoma. Blood 2021;137:637–45. [PubMed: 32870269]
15. Sakaguchi S, Sakaguchi N, Shimizu J, Yamazaki S, Sakihama T, Itoh M, et al. Immunologic tolerance maintained by CD25+ CD4+ regulatory T cells: their common role in controlling autoimmunity, tumor immunity, and transplantation tolerance. Immunol Rev 2001;182:18–32. [PubMed: 11722621]
16. Tanaka A, Sakaguchi S. Regulatory T cells in cancer immunotherapy. Cell Res 2017;27:109–18. [PubMed: 27995907]
17. Roncador G, Garcia JF, Garcia JF, Maestre L, Lucas E, Menarguez J, et al. FOXP3, a selective marker for a subset of adult T-cell leukaemia/lymphoma. Leukemia 2005;19:2247–53. [PubMed: 16193085]
18. Mittal S, Marshall NA, Duncan L, Culligan DJ, Barker RN, Vickers MA. Local and systemic induction of CD4+CD25+ regulatory T-cell population by non-Hodgkin lymphoma. Blood 2008;111:5359–70. [PubMed: 18305220]
19. Yang ZZ, Novak AJ, Stenson MJ, Witzig TE, Ansell SM. Intratumoral CD4+CD25+ regulatory T-cell-mediated suppression of infiltrating CD4+ T cells in B-cell non-Hodgkin lymphoma. Blood 2006;107:3639–46. [PubMed: 16403912]
20. Yang ZZ, Novak AJ, Ziesmer SC, Witzig TE, Ansell SM. Attenuation of CD8(+) T-cell function by CD4(+)CD25(+) regulatory T cells in B-cell non-Hodgkin's lymphoma. Cancer Res 2006;66:10145–52. [PubMed: 17047079]
21. Tzankov A, Meier C, Hirschmann P, Went P, Pileri SA, Dirnhofer S. Correlation of high numbers of intratumoral FOXP3+ regulatory T cells with improved survival in germinal center-like diffuse large B-cell lymphoma, follicular lymphoma and classical Hodgkin's lymphoma. Haematologica 2008;93:193–200. [PubMed: 18223287]
22. Carreras J, Lopez-Guillermo A, Fox BC, Colomo L, Martinez A, Roncador G, et al. High numbers of tumor-infiltrating FOXP3-positive regulatory T cells are associated with improved overall survival in follicular lymphoma. Blood 2006; 108:2957–64. [PubMed: 16825494]
23. Wahlin BE, Aggarwal M, Montes-Moreno S, Gonzalez LF, Roncador G, Sanchez-Verde L, et al. A unifying microenvironment model in follicular lymphoma: outcome is predicted by programmed death-1-positive, regulatory, cytotoxic, and helper T cells and macrophages. Clin Cancer Res 2010;16: 637–50. [PubMed: 20068089]
24. Yang ZZ, Kim HJ, Villasboas JC, Price-Troska T, Jalali S, Wu H, et al. Mass cytometry analysis reveals that specific intratumoral CD4(+) T cell subsets correlate with patient survival in follicular lymphoma. Cell Rep 2019;26: 2178–93. [PubMed: 30784598]
25. Kotecha N, Krutzik PO, Irish JM. Web-based analysis and publication of flow cytometry experiments. Curr Protoc Cytom 2010;Chapter 10:Unit10.17.
26. Wu H, Tang X, Kim HJ, Jalali S, Pritchett JC, Villasboas JC, et al. Expression of KLRG1 and CD127 defines distinct CD8(+) subsets that differentially impact patient outcome in follicular lymphoma. J Immunother Cancer 2021;9:e002662.
27. Hao Y, Hao S, Andersen-Nissen E, Mauck WM 3rd, Zheng S, Butler A, et al. Integrated analysis of multimodal single-cell data. Cell 2021;184:3573–87. [PubMed: 34062119]
28. Subramanian A, Tamayo P, Mootha VK, Mukherjee S, Ebert BL, Gillette MA, et al. Gene set enrichment analysis: a knowledge-based approach for interpreting genome-wide expression profiles. Proc Natl Acad Sci U S A 2005;102:15545–50. [PubMed: 16199517]

29. Yu G, Wang LG, Han Y, He QY. clusterProfiler: an R package for comparing biological themes among gene clusters. OMICS 2012;16:284–7. [PubMed: 22455463]
30. Collison LW, Vignali DA. In vitro Treg suppression assays. Methods Mol Biol 2011;707:21–37. [PubMed: 21287326]
31. Gubser C, Schmaler M, Rossi SW, Palmer E. Monoclonal regulatory T cells provide insights into T cell suppression. Sci Rep 2016;6:25758. [PubMed: 27210828]
32. Maurer MJ, Ghesquières H, Jais JP, Witzig TE, Haioun C, Thompson CA, et al. Event-free survival at 24 months is a robust end point for disease-related outcome in diffuse large B-cell lymphoma treated with immunochemotherapy. J Clin Oncol 2014;32:1066–73. [PubMed: 24550425]
33. Johnson WE, Li C, Rabinovic A. Adjusting batch effects in microarray expression data using empirical Bayes methods. Biostatistics 2007;8:118–27. [PubMed: 16632515]
34. Mondello P, Fama A, Larson MC, Feldman AL, Villasboas JC, Yang ZZ, et al. Lack of intrafollicular memory CD4+T cells is predictive of early clinical failure in newly diagnosed follicular lymphoma. Blood Cancer J 2021;11:130. [PubMed: 34267181]
35. Pesenacker AM, Bending D, Ursu S, Wu Q, Nistala K, Wedderburn LR. CD161 defines the subset of FoxP3+ T cells capable of producing proinflammatory cytokines. Blood 2013;121:2647–58. [PubMed: 23355538]
36. Povoleri GAM, Nova-Lamperti E, Scottà C, Fanelli G, Chen YC, Becker PD, et al. Human retinoic acid-regulated CD161(+) regulatory T cells support wound repair in intestinal mucosa. Nat Immunol 2018;19:1403–14. [PubMed: 30397350]
37. Palmer D, Guittard G, Patel S, Samelson LE, Restifo NP. Cish attenuates proximal TCR-signaling and CD8+ T cell immunity. J Immunother Cancer 2014;2:P32.
38. Stephens GL, McHugh RS, Whitters MJ, Young DA, Luxenberg D, Carreno BM, et al. Engagement of glucocorticoid-induced TNFR family-related receptor on effector T cells by its ligand mediates resistance to suppression by CD4+CD25+ T cells. J Immunol 2004;173:5008–20. [PubMed: 15470044]
39. Tinazzi E, Barbieri A, Rigo A, Patuzzo G, Beri R, Gerli R, et al. In rheumatoid arthritis soluble CD30 ligand is present at high levels and induces apoptosis of CD30(+)T cells. Immunol Lett 2014;161:236–40. [PubMed: 24447865]
40. Han L, Chen S, Chen Z, Zhou B, Zheng Y, Shen L. Interleukin 32 promotes Foxp3(+) treg cell development and CD8(+) T cell function in human esophageal squamous cell carcinoma microenvironment. Front Cell Dev Biol 2021;9:704853.
41. Yang XO, Pappu BP, Nurieva R, Akimzhanov A, Kang HS, Chung Y, et al. T helper 17 lineage differentiation is programmed by orphan nuclear receptors ROR alpha and ROR gamma. Immunity 2008;28:29–39. [PubMed: 18164222]
42. Koenen HJ, Smeets RL, Vink PM, van Rijssen E, Boots AM, Joosten I. Human CD25highFoxp3pos regulatory T cells differentiate into IL-17-producing cells. Blood 2008;112:2340–52. [PubMed: 18617638]
43. Müller J, Sperl B, Reindl W, Kiessling A, Berg T. Discovery of chromone-based inhibitors of the transcription factor STAT5. ChemBioChem 2008;9:723–7. [PubMed: 18247434]
44. Marri PR, Hodge LS, Maurer MJ, Ziesmer SC, Slager SL, Habermann TM, et al. Prognostic significance of pretreatment serum cytokines in classical Hodgkin lymphoma. Clin Cancer Res 2013;19:6812–9. [PubMed: 24141626]
45. Gause A, Jung W, Schmits R, Tschiersch A, Scholz R, Pohl C, et al. Soluble CD8, CD25 and CD30 antigens as prognostic markers in patients with untreated Hodgkin's lymphoma. Ann Oncol 1992;3:49–52. [PubMed: 1333270]
46. Yang Z-Z, Grote DM, Ziesmer SC, Manske MK, Witzig TE, Novak AJ, et al. Soluble IL-2Rα facilitates IL-2-mediated immune responses and predicts reduced survival in follicular B-cell non-Hodgkin lymphoma. Blood 2011; 118:2809–20. [PubMed: 21719603]
47. Veeramani S, Blackwell SE, Thiel WH, Yang ZZ, Ansell SM, Giangrande PH, et al. An RNA aptamer-based biomarker platform demonstrates high soluble CD25 occupancy by IL2 in the serum of follicular lymphoma patients. Cancer Immunol Res 2019;7:1511–22. [PubMed: 31383650]

48. Yang S, Xie C, Chen Y, Wang J, Chen X, Lu Z, et al. Differential roles of TNFα-TNFR1 and TNFα-TNFR2 in the differentiation and function of CD4(+)Foxp3(+) induced Treg cells in vitro and in vivo periphery in autoimmune diseases. Cell Death Dis 2019;10:27. [PubMed: 30631042]

Translational Relevance

Regulatory T cells (Treg) play an essential role in modulating immune function in cancer, but their role in splenic marginal zone lymphoma (SMZL) is not well described. In this study, we identified two Treg subsets, $CD161^+$ and $CD26^+$Tregs, in patients with SMZL with unique transcriptomic and phenotypic profiles and differing biological functions. These two Treg subsets have antithetical prognostic importance, in that patients with SMZL with more $CD161^+$Tregs have a superior outcome, whereas those in whom $CD26^+$Tregs are more abundant have an inferior outcome. Furthermore, we demonstrate that activation of the IL2/STAT5 pathway contributes to the induction of $CD26^+$Tregs and can be reversed by STAT5 inhibition. These findings not only support the biological relevance of Treg subsets in SMZL, but also suggest that modulating the balance of Treg subsets by inhibiting IL2/STAT5 signaling, thereby promoting the $CD161^+$Treg phenotype, may improve the clinical outcome of patients with SMZL.

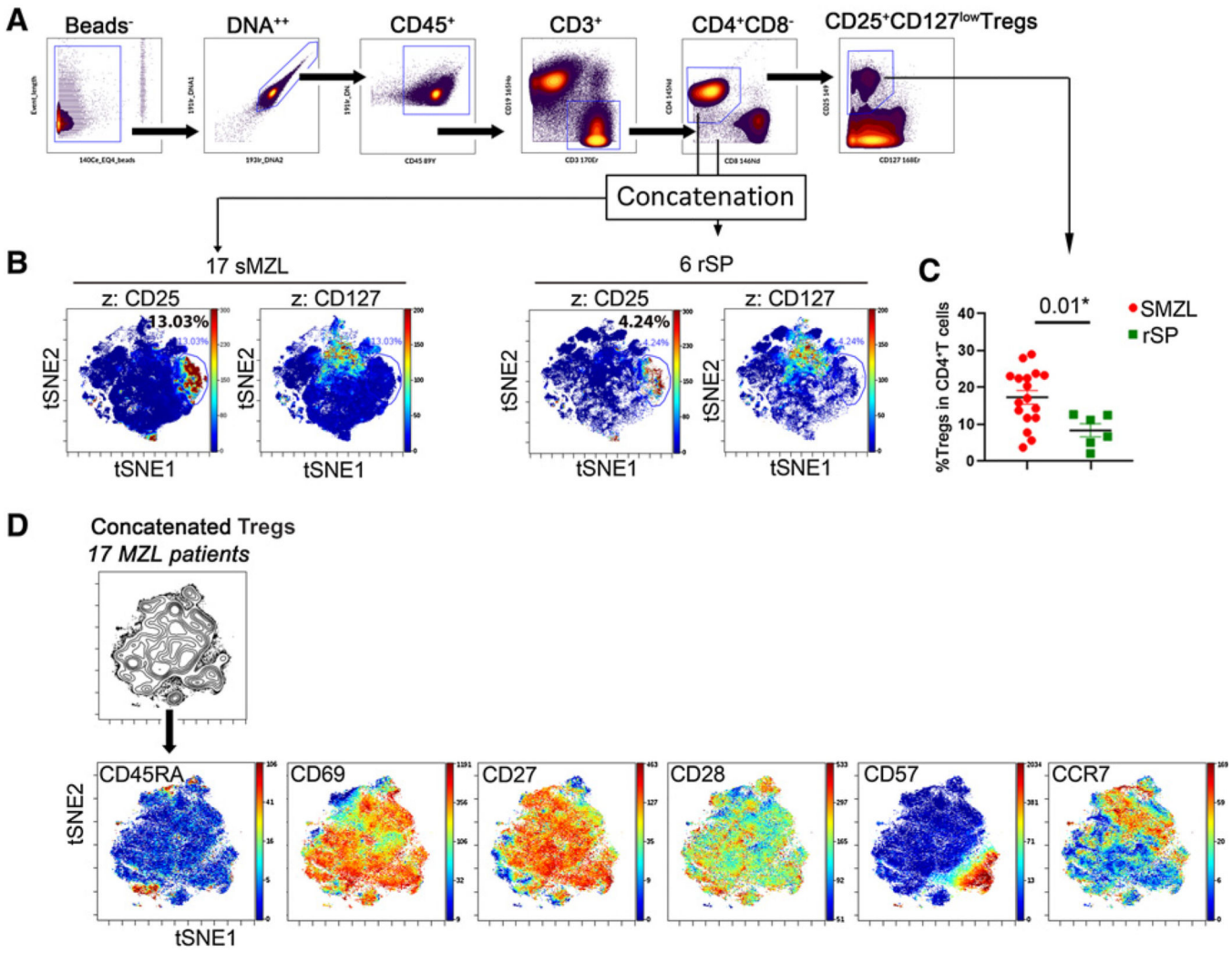

Figure 1.

Intratumoral Tregs are enriched in patients with SMZL. **A,** Gating strategy for $CD4^{+}CD25^{+}CD127^{low}$Tregs showing in a representative sample of a patient with SMZL. **B,** The tSNE plots show the expression of CD25 and CD127 to define Tregs. **C,** Graph showing percentage of Tregs ($CD4^{+}CD25^{+}CD127^{low}$) in $CD4^{+}$T cells in patients with MZL ($n = 17$). For parametric data comparisons, the unpaired t test was used here (t value = 2.709; degree of freedom = 21). **D,** Series of tSNE maps performed on concatenated Tregs files (17 SMZL) showing expression of T-cell markers on Tregs.

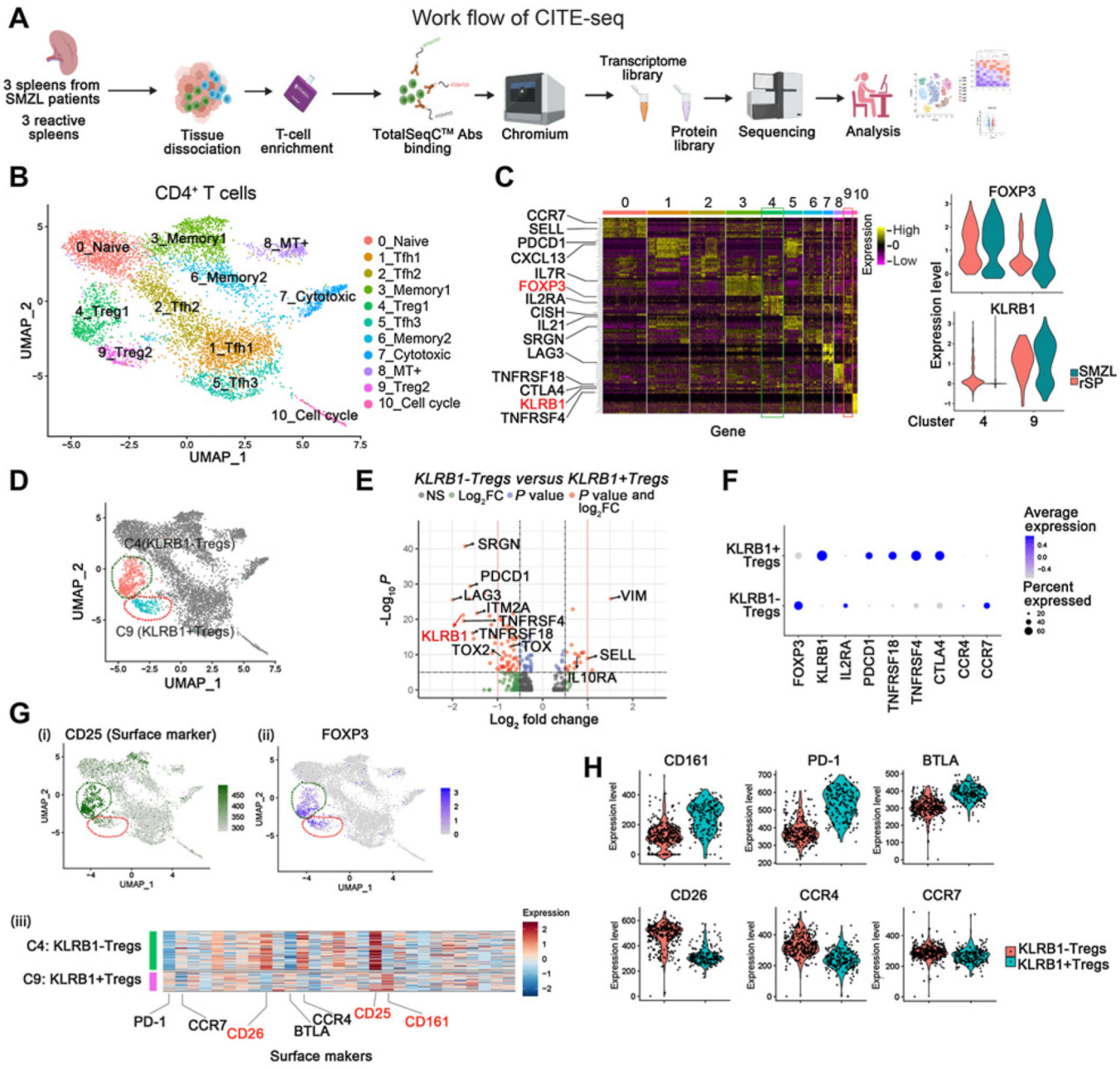

Figure 2.

Multi-omics analysis of CD4$^+$T cells identifies Treg subsets in SMZL. **A,** Schematic representation of T cell enrichment strategy and CITE-seq experimental design. **B,** UMAP plot visualization of intratumoral CD4$^+$T cell clusters detected in rSP (n = 3) and SMZL (n = 3), and clusters are colored and distinctively labeled. **C,** Heatmap showing relative expression of marker genes of each cluster (left). Violin plots showing the *FOXP3* and *KLRB1* expression levels in cluster4 and cluster9 (right). **D,** Diffusion map of FOXP3$^+$Treg subsets (Cluster4: *KLRB1*-Tregs, Cluster9: *KLRB1*+Tregs) in CD4$^+$T cells in patients with SMZL and rSP individuals. **E,** Volcano plot of CITE-seq transcriptome data displaying the pattern of gene expression values for Cluster4 (*KLRB1*-Tregs) versus

Cluster9 (*KLRB1*+Tregs) in SMZL samples ($n = 3$). Significantly differentially expressed genes ($|\log_2 FC| \geq 0.5$, adjusted P value ≤ 10–6) are shown in red, with the red dotted lines representing the boundary for identifying very significantly up- or downregulated genes ($|\log_2 FC| \geq 1.0$). **F,** Dot plot showing diverse gene expression in *KLRB1*+Tregs and *KLRB1*-Tregs in three SMZL samples. **G,** (i) Expression of CD25 (surface marker) was shown by using UMAP plot. (ii) Expression of *FOXP3* was shown by using UMAP plot. (iii) Heatmap showing relative expression of surface markers of Cluster4 (KLRB1-Tregs) and Cluster9 (*KLRB1*+Tregs). These three figures show data from rSP ($n = 3$) and SMZL ($n = 3$). **H,** Violin plots showing the CD161 (encoded by *KLRB*1 gene), CD26, PD-1, CCR4, BTLA, and CCR7 expression levels in *KLRB1*+Tregs and *KLRB1*-Tregs from rSP ($n = 3$) and SMZL ($n = 3$).

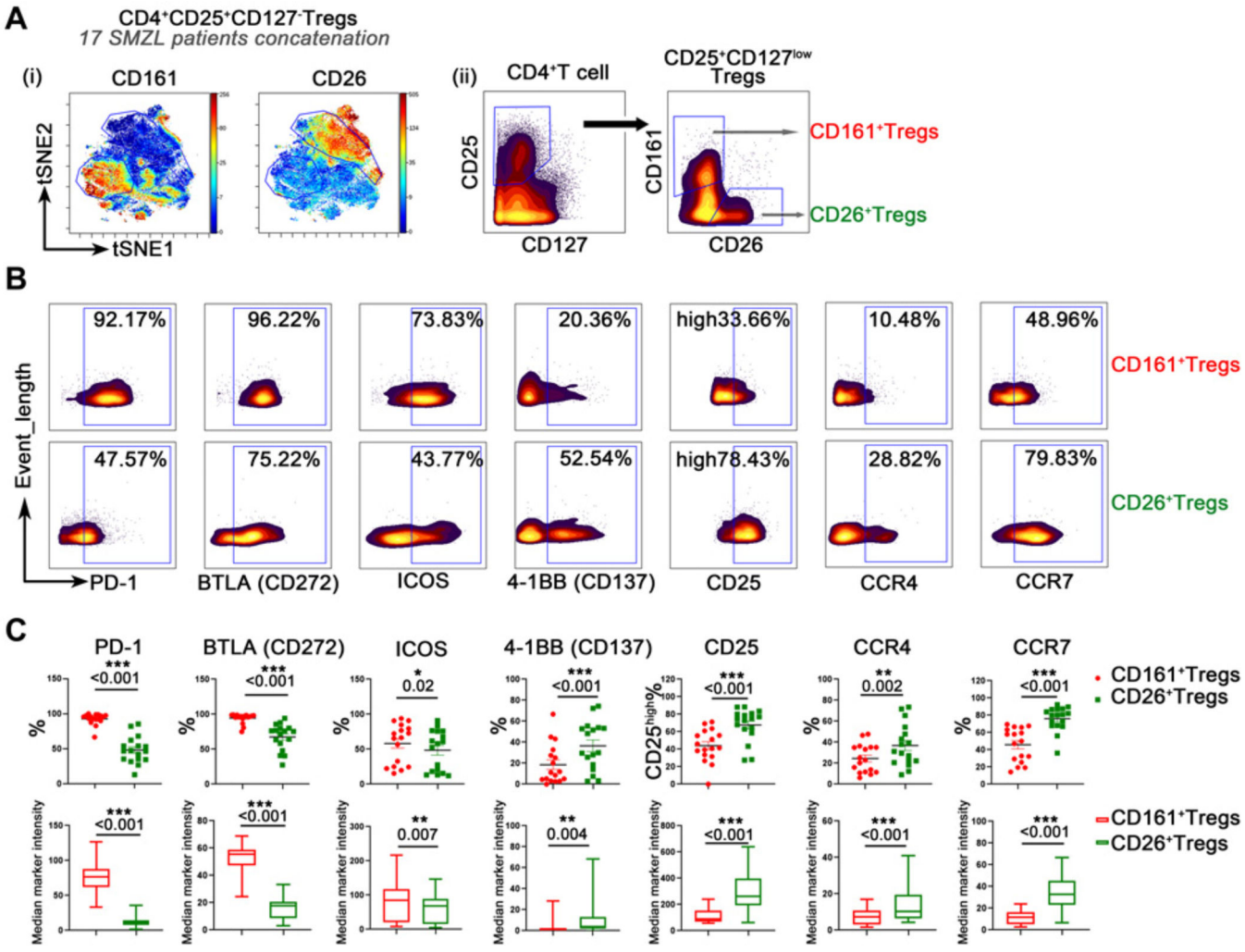

Figure 3.

CD161 and CD26 expression defines Treg subsets. **A,** (i) tSNE plots showing the expression of CD161 and CD26 on the concatenated Treg file to define Treg subsets (CD161^{+}Tregs and CD26^{+}Tregs); (ii) Plots from a representative sample of patient with SMZL showing gate strategy for CD161^{+}Tregs and CD26^{+}Tregs. **B,** Series of plots showing expression of surface markers on CD161^{+}Tregs and CD26^{+}Tregs in a representative sample of patient with SMZL. **C,** Graphs summarizing the percentages and median marker intensity of surface markers on CD161^{+}Tregs and CD26^{+}Tregs in patients with SMZL (n = 17). Paired t tests were used for comparisons of CCR4% and the median marker intensity of CCR7, ICOS, and BTLA. For other parameter comparisons, the nonparametric Wilcoxon matched-pairs signed-rank test was used.

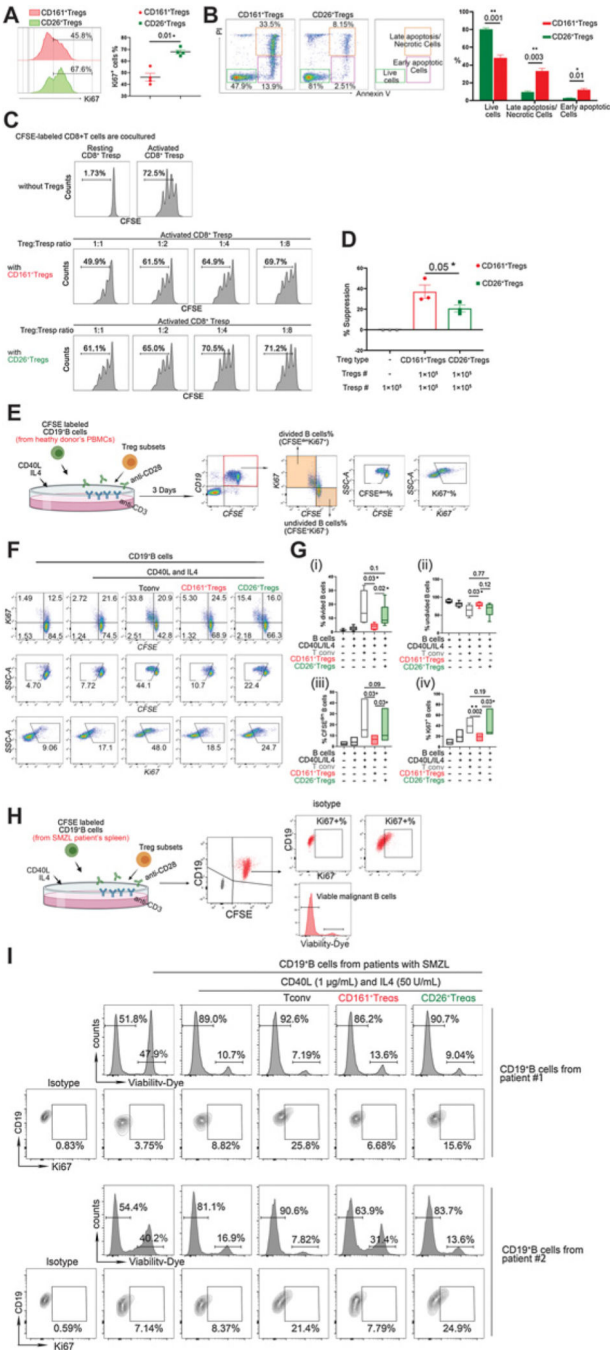

Figure 4.

CD161$^+$ and CD26$^+$Tregs exhibit differing capacities for cell proliferation, survival, and immune suppression. **A,** Proliferation of Treg subsets, isolated from PBMCs of healthy donors, was evaluated by detecting the percentage of Ki67$^+$ cells and is shown in representative histograms (left). The Ki67$^+$ population in CD26$^+$Tregs increased significantly compared with CD161$^+$ Tregs (right); paired *t* test was used here ($n = 4$ individual healthy donors). **B,** Treg subsets, isolated from PBMCs of healthy donors, were labeled with Annexin V (AnV) and propidium iodide (PI) after 72 hours of incubation;

the percentages of necrotic cells (AnV^+PI^+), early apoptotic cells (AnV^+PI^-), and live cells (AnV^-PI^-) are shown in the representative plots (left and central panel). The percentage of live cells (AnV^-PI^-) was significantly lower in $CD161^+$Tregs than that of $CD26^+$Tregs. In contrast, the percentage of early apoptotic (AnV^+PI^-) and late apoptotic/necrotic (AnV^+PI^+) cells was significantly higher in $CD161^+$Tregs than $CD26^+$Tregs (right); paired *t* test was used here ($n = 3$ individual healthy donors). **C,** Representative plots showing the percentage of divided $CD8^+$T (T response cells, Tresp) cells when cocultured with Treg subsets at different ratios (Treg subsets:Tresp = 1:1–8); cells were isolated from PBMCs of a healthy donor. **D,** Suppressive function was calculated [%Suppressive = 1 – (%proliferating cells with Treg present/%proliferating cells without Treg present)], and the suppressive function of $CD161^+$Tregs on $CD8^+$T cells is significantly stronger; paired *t* test was used here ($n = 3$ individual healthy donors). **E,** Schematic representation of Treg subsets co-cultured with B cells experimental design. **F,** Representative plots of CFSE-labeled B cells co-cultured with different T-cell subsets in the presence of CD40L, IL4, functional anti-CD3, and anti-CD28 antibodies (CD40 L and IL4 are for B-cell activation, functional anti-CD3 and anti-CD28 antibodies are for T-cell activation); cells were isolated from PBMCs of healthy donors. **G,** Proliferation ability of B cells was detected. (i) Graph shows percentage of divided B cells when cocultured with Tconv and Treg subsets. (ii) Graph shows percentage of undivided B cells when cocultured with Tconv and Treg subsets. (iii) Graph shows percentage of $CFSE^{dim}$ B cells when cocultured with Tconv and Treg subsets. (iv) Graph shows percentage of $Ki67^+$ B cells when cocultured with Tconv and Treg subsets. Compared with $CD26^+$Tregs and conventional T cells, $CD161^+$Tregs show significant suppression on the percentage of divided cells and $CFSE^{dim}$ cells and Ki67 expression of Bcells;paired *t* test was used here ($n = 6$, the experiments were conducted on the cells that were isolated from 6 individual healthy donors). **H,** Schematic representation of Treg subsets co-cultured with malignant B cells experimental design. **I,** $CD19^+$B cells from spleen of 2 patients with SMZL cocultured with Treg subsets (from healthy donor PBMCs) at 1:1 ratio. Viability (%viability-dye negative cells) and proliferation ability (%Ki67+ cells) of malignant B cells was detected by FCM.

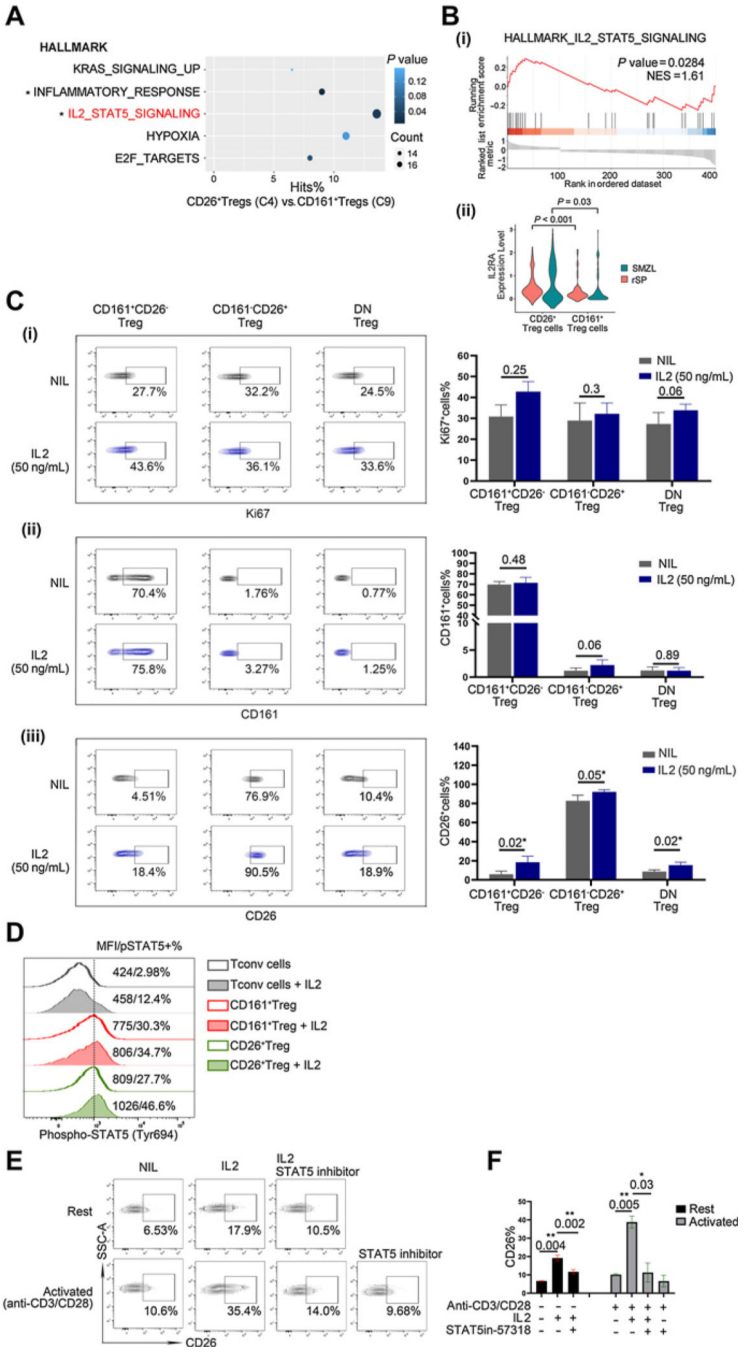

Figure 5.

IL2 promotes the development of CD26^{+}Tregs with the involvement of STAT5. **A,** Scatterplot of enriched GSEA pathways. *Y*-axis represents pathway name, and *X*-axis represents the percentage of gene hits. Size and color of each bubble represent the number of differentially expressed genes enriched in the pathway and *P* value, respectively. **B,** (i) The enrichment score curve showing alteration of signaling pathways involving IL2/STAT5 pathway in Treg subsets from patients with SMZL, $n = 3$. The enrichment score normalized (NES) greater or less than zero indicates an upregulation or downregulation,

respectively. These data were generated using GSEA. (ii) Violin plot showing the IL2RA gene expression levels in $CD26^{+}$Tregs and $CD161^{+}$Tregs (SMZL: $P = 0.03$; rSP: $P < 0.001$). **C,** (i) Contour plots showing expression of Ki67 in each Treg subset in the presence of IL2. The percentages of $Ki67^{+}$ cells induced by IL2 were summarized in the graph; Wilcoxon matched-pairs signed rank test and paired *t* test were used here ($n = 3$). (ii) Contour plots showing expression of CD161 on each Treg subset in the presence of IL2. The percentages of $CD161^{+}$ cells induced by IL2 are summarized in the graph; paired *t* test was used here ($n = 3$). (iii) Contour plots showing expression of CD26 on each Treg subset in the presence of IL2. The percentages of $CD26^{+}$ cells induced by IL2 are summarized in the graph; paired *t* test was used here ($n = 3$). The experiments were conducted on the cells that were isolated from three individual healthy donors. **D,** Histogram plots show the STAT5-Tyr694 phosphorylation in $CD161^{+}$Tregs, $CD26^{+}$Tregs with or without IL2 treatment (50 ng/mL for 20 minutes); Treg subsets were isolated from PBMCs of healthy donors. **E,** Contour plots showing expression of CD26 on DN Tregs ($CD161^{-}CD26^{-}$) in the presence of IL2 (50 ng/mL) and with or without STAT5 inhibitor (57318; 50ng/mL), Treg subsets were isolated from PBMCs of healthy donors. **F,** The percentages of $CD26^{+}$Tregs induced by IL2 plus STAT5 inhibitor (57318) are summarized in the graphs ($n = 3$ individual healthy donors).

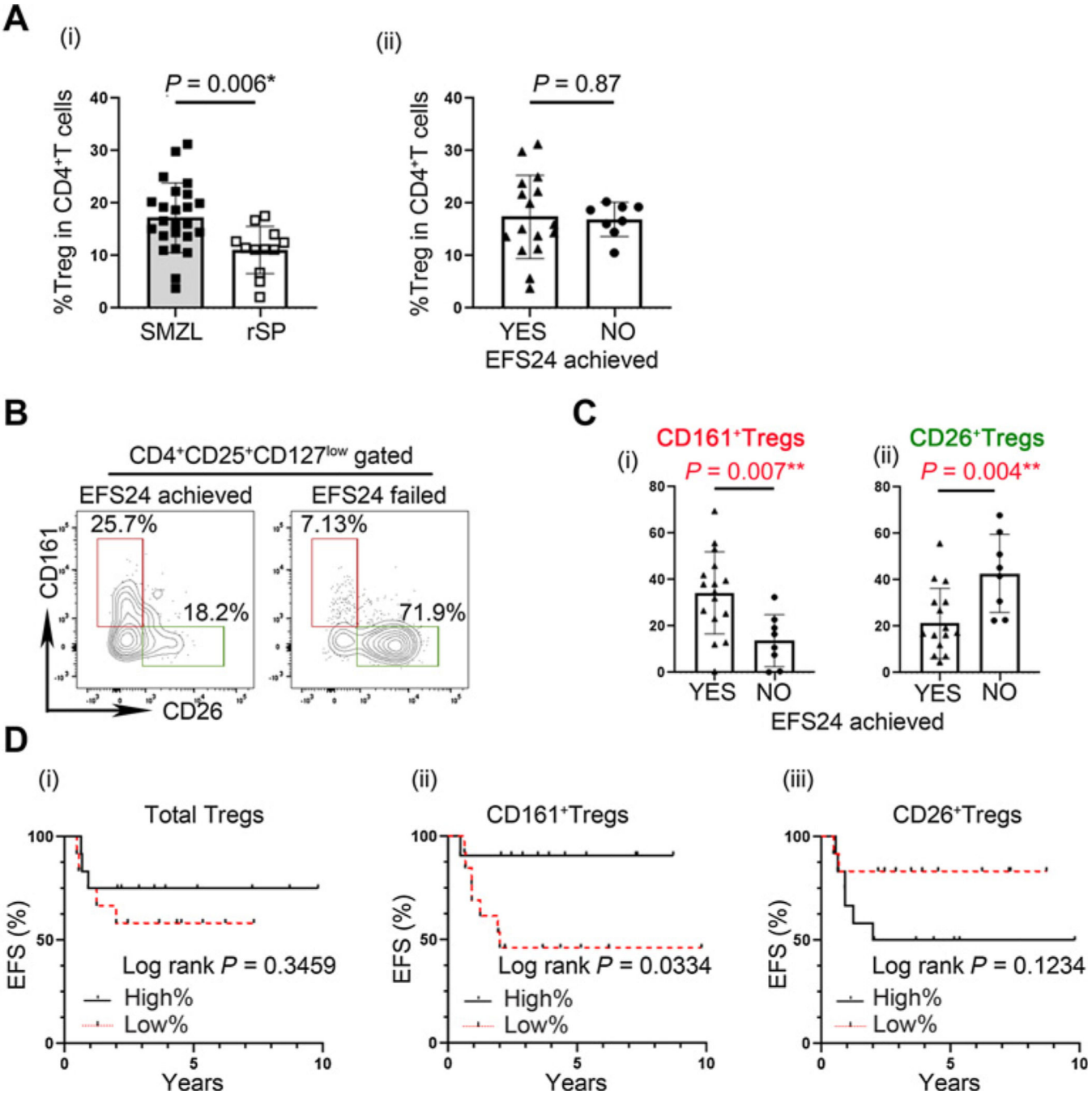

Figure 6.

Intratrumoral CD161^{+}Tregs and CD26^{+}Tregs differentially correlate with patient outcomes in SMZL. **A,** (i) Percentage of total Tregs in CD4^{+}T cells in patients with SMZL (n = 24), rSP (n = 12), for nonparametric data comparison; Mann–Whitney was used here. (ii) Graph showing percentages of total Tregs in 2 patient groups. Patients with SMZL were grouped using 24-month event-free survival (EFS24, achieved vs. failed; n = 24), for parametric data comparison, unpaired t test was used here (t value = 0.1679, degree of freedom = 22). **B,** Representative plots showing CD161 and CD26 on Treg in spleen of EFS24 achieved and

failed patients with MZL. **C,** (i) Graph showing percentages of $CD161^{+}$Treg in 2 patient groups. Patients with SMZL were grouped using 24-month event-free survival (EFS24, achieved vs. failed; $n = 24$), for parametric data comparison, unpaired t test was used here (t value = 2.995, degree of freedom = 22). (ii) Graph showing percentages of $CD26^{+}$Treg in 2 patient groups. Patients with SMZL were grouped using 24-month event-free survival (EFS24, achieved vs. failed; $n = 24$), for parametric data comparison, unpaired t test was used here (t value = 3.178, degree of freedom = 22). **D,** Kaplan–Meier curves for EFS of patients with SMZL ($n = 24$) by the percentages of Total Tregs (i), $CD161^{+}$Tregs (ii), and $CD26^{+}$Tregs (iii) with a cutoff of median value; log-rank test was used here.